Chapter 23

MODIS&VIIRS LAI/FPAR

Jiabin Pu, Yuri Knyazikhin and Ranga B. Myneni
Department of Earth and Environment, Boston University, Boston, MA, United States

1. Introduction: product definition and importance

The leaf area index (LAI) measures the half leaf area per unit ground area, presenting the vegetation canopy structural and functional characteristics (Chen and Black, 1992; Knyazikhin et al., 1998). The Faction of incident Photosynthetically Active Radiation (FPAR) is derived across the 400–700 nm range of chlorophyll absorption and characterizes the fraction of sunlight absorbed by vegetation for photosynthesis (Knyazikhin et al., 1998). These two metrics are widely used in the fields of land-atmosphere energy balance, plant productivity, carbon and water cycle, climate change, and agricultural and forestry management (Chen and Black, 1992; Chen et al., 2019; Zhu et al., 2016; Knyazikhin et al., 1998; Skidmore and Pettorelli, 2015).

As components of climate data records (CDRs) and essential climate variables (ECVs), long-term consistent LAI/FPAR datasets provide the essential basis for monitoring vegetation dynamics due to climate variability and human activities (GCOS, 2011, 2016; Bojinski et al., 2014). The Moderate Resolution Imaging Spectroradiometer (MODIS) on NASA's Terra and Aqua platforms, provides LAI/FPAR datasets for long-term environmental monitoring and climate research and has been a cornerstone in Earth observation since the early 2000s (Knyazikhin, 1999; Myneni and Park, 2015; Yan et al., 2016a). Visible Infrared Imaging Radiometer Suite (VIIRS), on the Suomi National Polar-orbiting Partnership (S-NPP) and NOAA-20 satellites, was developed to extend the MODIS long-term LAI/FPAR time series at the same spatial and temporal resolution as MODIS (Yan et al., 2018; Justice et al., 2013; Roman et al., 2024). In general, FPAR values vary by illumination condition. To standardize FPAR across illumination conditions, the MODIS&VIIRS products provide FPAR under direct solar illumination for the solar zenith angle at a given time of observation. MODIS and VIIRS LAI/FPAR products together support a wide range of applications, including assessing vegetation productivity, understanding energy exchanges, and studying the global carbon cycle (Tang et al., 2013; Mariano et al., 2018; Chen et al., 2019, 2022). Also, these datasets are fundamental for improving climate models and tracking changes in terrestrial ecosystems (Winkler et al., 2024).

2. Product characteristics

The Collection 6.1 (C61) MODIS LAI/FPAR products (MOD15A2H and MYD15A2H) are derived from the Terra/Aqua observations and provide global coverage at a spatial resolution of 500 m and a temporal frequency of 8 days. FPAR is estimated at 10:30 a.m. and 1:30 p.m. Local Solar Time (LCT) for MOD15A2H and MYD15A2H, respectively. The projection used for the LAI/FPAR products product is the sinusoidal grid tiling system (Myneni and Park, 2015; Yan et al., 2016a). The data is distributed in hierarchical data format (HDF). Each file contains six science data sets (SDSs), namely FPAR, standard deviation of FPAR (FparStdDev) and LAI (LaiStdDev), algorithm path (FparLai_QC), and "other quality assessment" (FparExtraQC). Details on the file structure and contents are available in Myneni and Park (2015).

NASA SNPP-VIIRS and JPSS-VIIRS Collection 2 (C2) LAI/FPAR products (VNP15A2H/VJ115A2H) aimed to provide a critical bridge between MODIS and VIIRS. The dataset is being generated by the MODIS LAI/FPAR algorithm (Yan et al., 2018; Knyazikhin and Myneni, 2018). An adjustment technique for the algorithm was developed to ensure consistency in retrievals generated from sensors of different resolutions and spectral band compositions (Ganguly et al., 2008a, 2008b; Chen et al., 2017). Same as MODIS, each file includes six SDSs (Fpar, Lai, FparStdDev, LaiStdDev, FparLai_QC, FparExtra_QC), which are distributed in the HDF-EOS5 (H5).

Handbook of Satellite Land Products. https://doi.org/10.1016/B978-0-443-21485-1.00023-6
Copyright © 2026 Elsevier Inc. All rights are reserved, including those for text and data mining, AI training, and similar technologies.

TABLE 23.1 Data description of MODIS&VIIRS LAI/FPAR products.

Temporal coverage	MOD15AH Collection 6.1 (February 18, 2000—Current) MYD15A2H Collection 6.1 (July 14, 2002—Current) VNP15A2H Collection 2 (January 17, 2012—Current) VJ115A2H Collection 2 (January 1, 2018—Current)
Temporal resolution	8 days
Area	Global vegetation area
Projection	Sinusoidal
Spatial resolution	500m
Valid range	0–70 for LAI and 0–100 for FPAR
Multiply by scale factor	0.1 for LAI and 0.01 for FPAR
Science data sets (SDSs)	FPAR or Fpar (FPAR retrievals) LAI or Lai (LAI retrievals) FparStdDev (standard deviation of FPAR) LaiStdDev (standard deviation of LAI) FparLai_QC (algorithm path and atmosphere conditions) FparExtra_QC (atmosphere conditions)
File format	HDF for MOD15A2H/MYD15A2H HDF5 for VNP15A2H/VJ115A2H

However, compared to MODIS LAI/FPAR products that are produced from both morning (Terra, MOD15A2H) and afternoon (Aqua, MYD15A2H) observations, the C2 VIIRS LAI/FPAR are produced from the afternoon observation only (1:30 p.m. LCT). The characteristics of the MODIS&VIIRS LAI/FPAR can be found in Table 23.1.

3. Product algorithm

The daily MODIS&VIIRS LAI/FPAR retrieval algorithm inputs Bidirectional Reflectance Factor (BRF) at the red and NIR spectral bands, their uncertainties, sun-sensor geometry, and biome classification map and retrieves the LAI and FPAR for each satellite pixel. The retrieval technique consists of the main algorithm, which is based on the radiative transfer model, and the backup algorithm that uses the empirical relationship between NDVI and LAI and FPAR. The main algorithm compares observed and modeled spectral BRF with those evaluated from the model-based entries stored in a look-up-table (LUT) for a suite of canopy structures and soil patterns that represent an expected range of typical conditions for a given biome type. All canopy/soil patterns values for which modeled and observed BRFs differ within a specified uncertainty level are acceptable solutions. FPAR is also calculated for each acceptable solution. The mean values of LAI and FPAR averaged over all acceptable solutions and their dispersions are taken as solutions and retrieval uncertainties. When this method fails to localize a solution, the backup method is utilized (Knyazikhin et al., 1998; Knyazikhin, 1999; Myneni and Park, 2015). The daily retrievals are composited over an 8-day period by selecting the LAI and FPAR pair corresponding to the maximum FPAR value generated by the main algorithm. The backup algorithm retrievals are selected only when no main algorithm retrievals are available during the 8-day compositing period. Analyses of the algorithm performance indicate that best quality, high-precision retrievals are obtained from the main algorithm (Myneni et al., 2002; Yang et al., 2006; Yan et al., 2016a, 2016b).

In the case of dense canopies, the reflectances saturate, therefore, are weakly sensitive to changes in canopy properties. The reliability of parameters retrieved under the condition of saturation is lower than that generated by the main algorithm using unsaturated BRF. Such retrievals are flagged. The algorithm path, therefore, is the key quality assessment flag that provides information about the overall quality of the LAI/FPAR. The QA variables also provide information about the cloud state, aerosol load, and the presence of snow, which are inherited from the upstream BRF product.

4. Product assessment

The global spatial distribution of MODIS and VIIRS annual average LAI and FPAR over the overlap-year period between 2018 and 2023 are both shown in Figs. 23.1 and 23.2. For both LAI and FPAR, there is no visually distinguishable difference between MODIS C61 and the

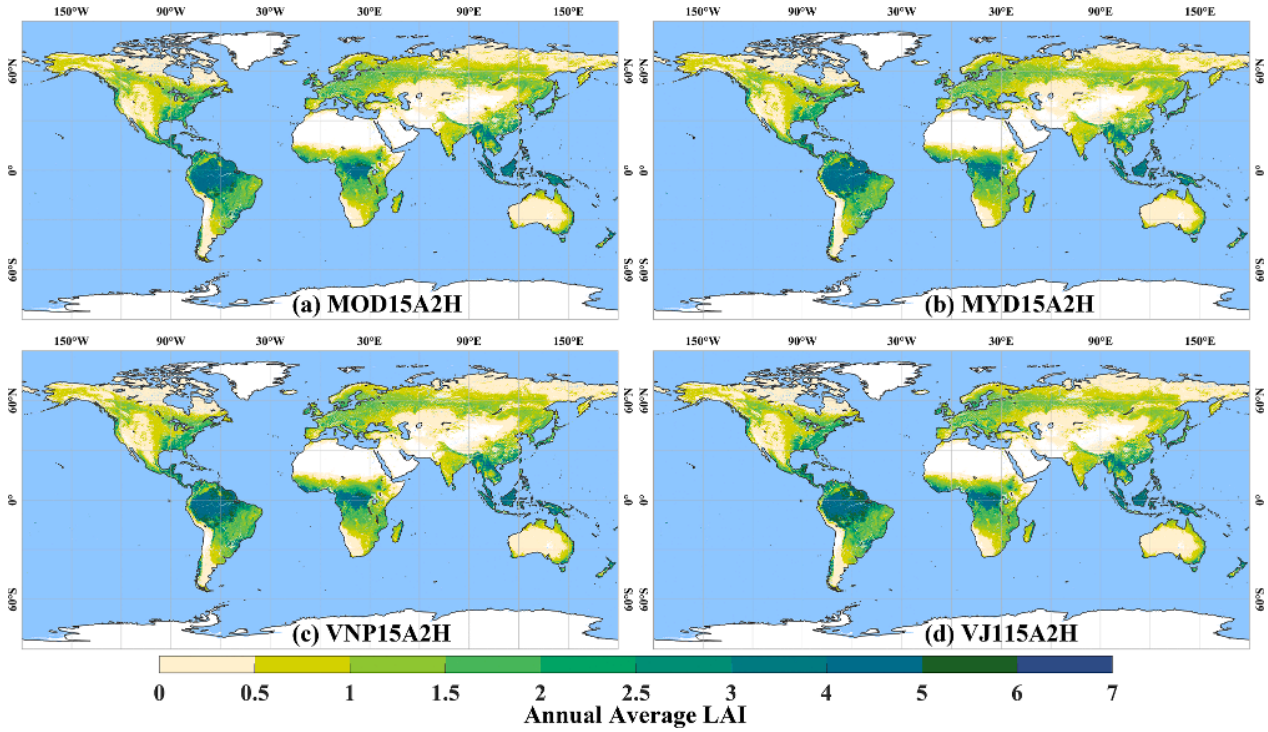


FIGURE 23.1 Annual LAI averaged over the overlap year study period (2018–23) for MODIS&VIIRS LAI products. (a) MOD15A2H, (b) MYD15A2H, (c) VNP15A2H, and (d) VJ115A2H. ***Map lines delineate study areas and do not necessarily depict accepted national boundaries.***

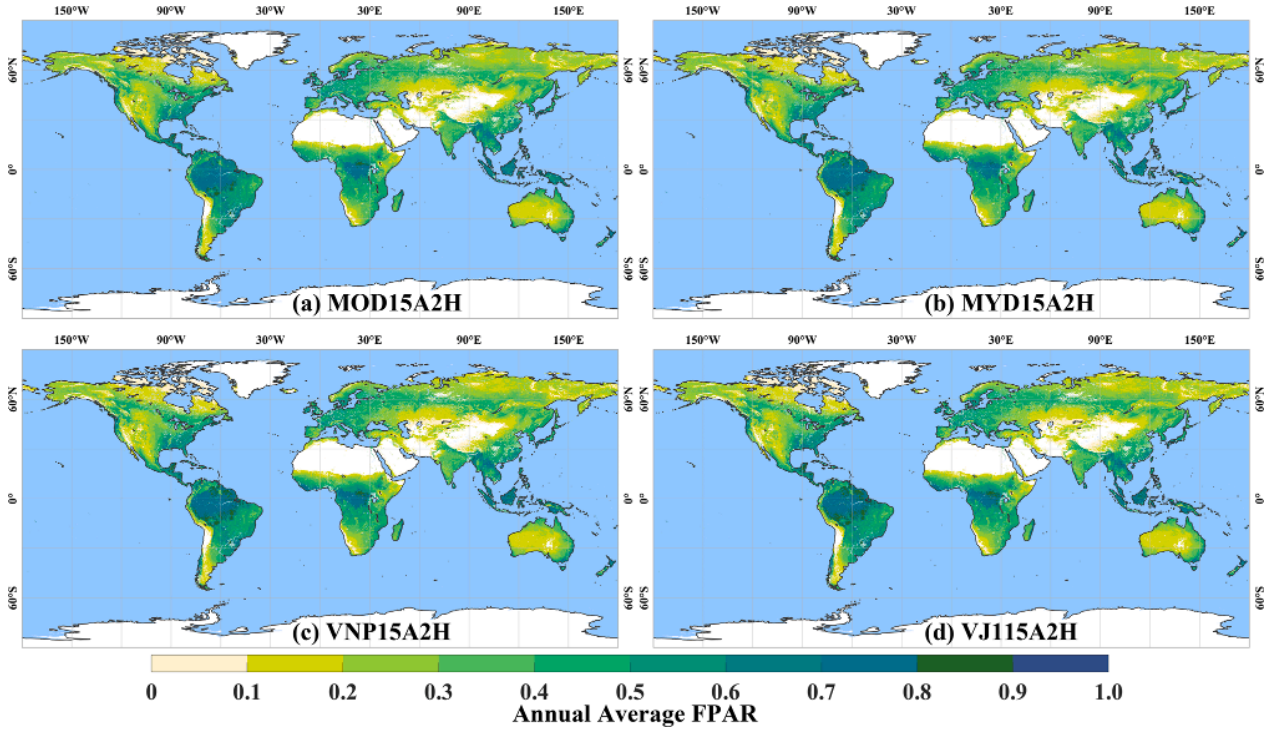


FIGURE 23.2 Same as Fig 23.1 but for FPAR. Annual FPAR averaged over the overlap year study period (2018–23) for MODIS&VIIRS FPAR products. ***Map lines delineate study areas and do not necessarily depict accepted national boundaries.***

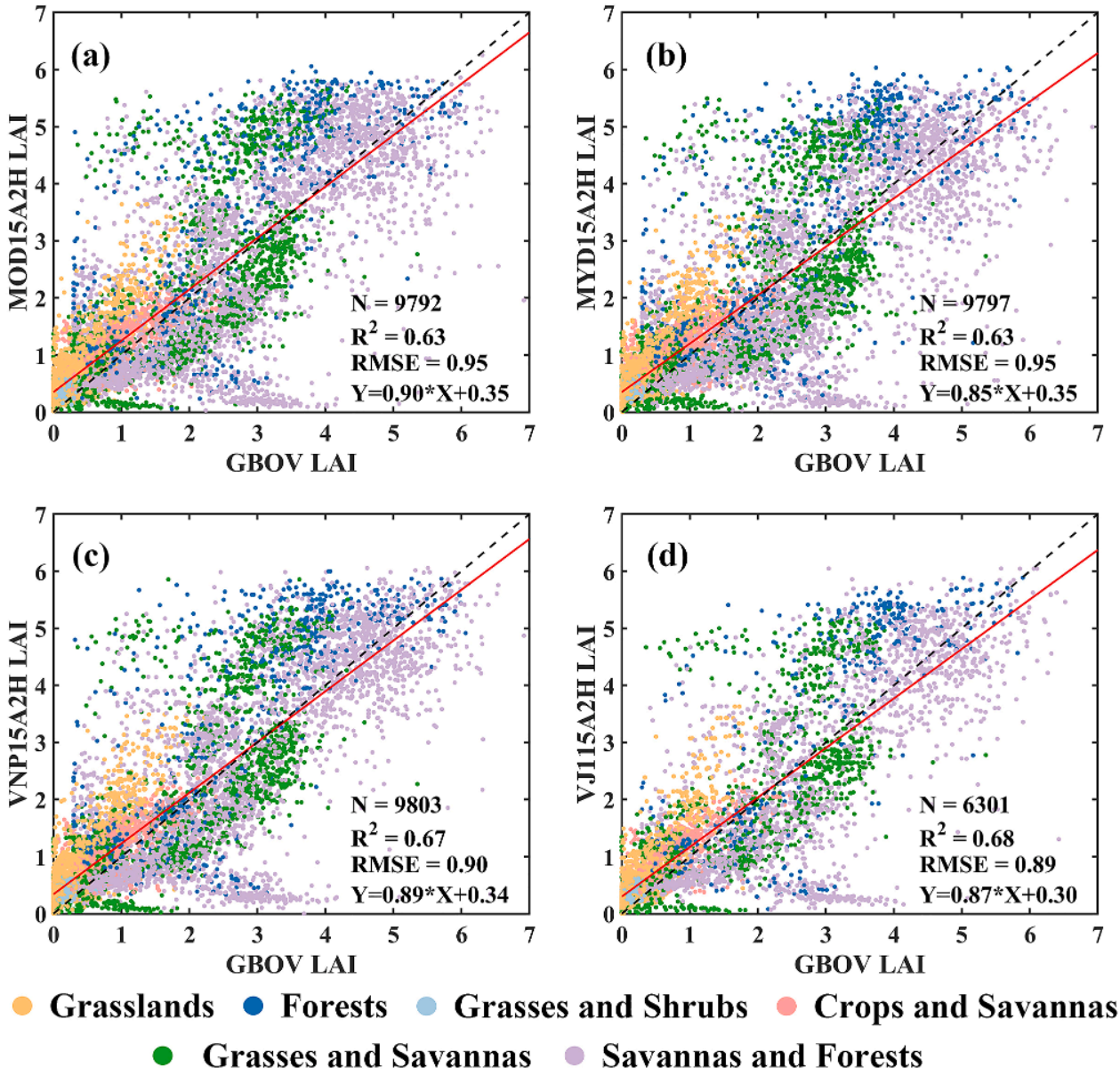


FIGURE 23.3 Validation of MODIS&VIIRS LAI products with GBOV ground-based measurements (29 sites). Symbol colors correspond to different biome types.

new VIIRS C2 (will discuss later). The products from the four sensors exhibit similar patterns. The global annual average LAIs are around 1.24–1.31, and the numbers for FPAR are all around 0.36. The vegetated areas that LAI less than 1 range from 53.66% to 55.32%, which represents that there are large regions for sparse vegetation. And the FPARs are around 0.21–0.22 for the same sparse vegetated area. Meanwhile, the vegetated area with LAI greater than 4 (mainly for forests) ranges from 6.09% to 8.01%, and the FPARs are around 0.75–0.77 for this density vegetation area. Notably, the FPAR increased not much as the LAI increased, which means the relationship between LAI and FPAR showed a saturated situation over the high-LAI vegetated region.

Figs. 23.3 and 23.4 present comparisons of Copernicus ground-based measurements for validation (GBOV) LAI/FPAR with MODIS C61 and VIIRS C2 LAI/FPAR, respectively (Brown et al., 2020). Our analysis indicates the consistency between uncertainties in VIIRS and MODIS LAI/FPAR retrievals, that is, comparable values of R2 and RMSE when compared to ground truth data (Tables 23.2 and 23.3). Notably, both products showed a

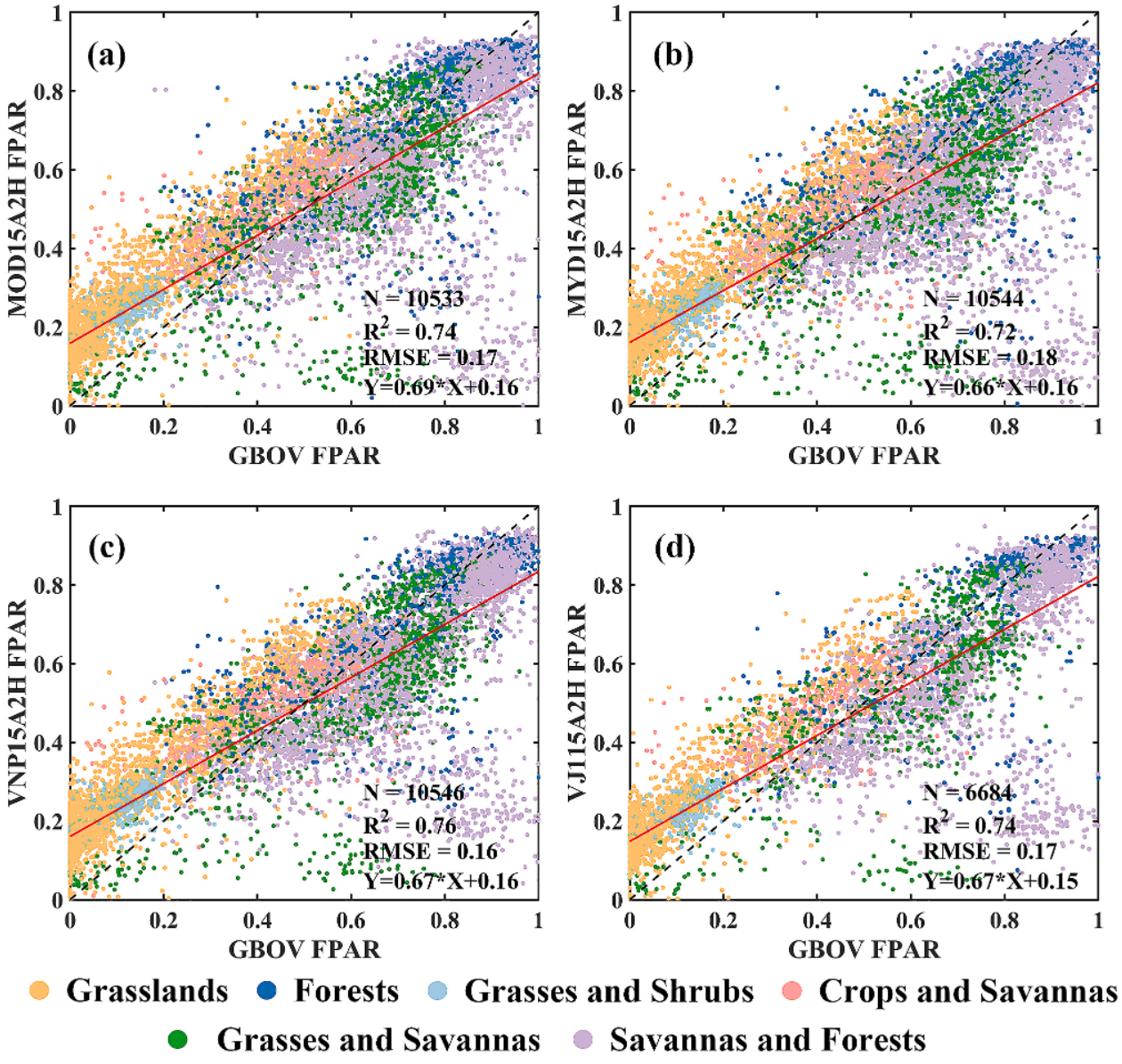


FIGURE 23.4 Same as Fig. 23.3 but for FPAR. Validation of MODIS&VIIRS FPAR products with GBOV ground-based measurements.

tendency to overestimate low LAI/FPAR and underestimate high FPAR. Moreover, VIIRS C2 outperformed MODIS C61 in terms of LAI retrieval accuracy, with a decrease in RMSE from 0.95 /0.95 (MOD15A2H/MYD15A2H) to 0.90 /0 0.89 (VNP15A2H/VJ115A2H) and an increase in R2 from 0.63 /0.63 to 0.67 /0.67. Similarly, for FPAR, the R2 increased from 0.74 /0.72 to 0.76 /0.74. Note that the resulting estimate should technically be referred to as the plant area index (PAI) since in situ measurements may be sensitive to all elements of the canopy (Brown et al., 2021). Studies have demonstrated that the PAI may overestimate LAI in certain scenarios, e.g., forests (Brown et al., 2021), which is illustrated in Fig. 23.3 (overestimate LAI for forest sites) and Table 23.2 (higher RMSE).

As SNPP-VIIRS and JPSS-VIIRS are designed to expand the long-term MODIS LAI/FPAR time series from Terra and Aqua missions under the background that MODIS will be retired in the not long future, it is crucial to ensure consistency between MODIS and VIIRS LAI/FPAR products on a global scale (Xu et al., 2018; Yan et al., 2018, 2021). Fig. 23.5 displays the global spatial

TABLE 23.2 Comparison of MODIS LAI and VIIRS LAI over GBOV sites.

Biome type	Site	R^2 MOD	RMSE MOD	R^2 MYD	RMSE MYD	R^2 VNP	RMSE V
Grasslands	CPER	0.34	0.37	0.35	0.36	0.35	0.37
	KONA	0.84	0.74	0.84	0.76	0.87	0.81
	MOAB	0.06	0.21	0.03	0.22	0.05	0.21
	ONAQ	0.13	0.25	0.14	0.25	0.13	0.25
	SPER	0.20	0.27	0.20	0.25	0.20	0.25
	STER	0.59	0.36	0.59	0.36	0.59	0.39
	WOOD	0.72	0.85	0.74	0.79	0.74	0.87
Forests	HARV	0.55	1.41	0.50	1.43	0.58	1.35
	TALL	0.55	1.42	0.57	1.36	0.64	1.36
	TUMB	0.65	0.94	0.72	0.85	0.69	0.65
Grass and shrubs	JORN	0.10	0.23	0.09	0.23	0.10	0.24
	VALE	0.21	0.28	0.17	0.28	0.20	0.30
Crops and savannas	BLAN	0.55	0.44	0.53	0.44	0.54	0.44
	LAJA	0.40	0.50	0.32	0.48	0.41	0.48
Grass and savannas	GUAN	0.26	1.85	0.15	1.73	0.21	1.63
	JERC	0.57	0.77	0.53	0.83	0.61	0.74
	LITC	0.41	0.91	0.20	0.82	0.08	0.89
	NIWO	0.02	0.51	0.02	0.50	0.01	0.53
Savannas and forests	BART	0.40	1.54	0.37	1.55	0.44	1.53
	DELA	0.70	0.94	0.63	1.00	0.76	0.82
	DSNY	0.36	0.95	0.22	1.09	0.39	0.88
	HAIN	0.49	1.54	0.58	1.34	0.64	1.24
	ORNL	0.62	1.06	0.58	1.12	0.67	0.99
	OSBS	0.22	0.95	0.15	0.92	0.24	0.91
	SCBI	0.78	0.97	0.75	1.05	0.87	0.76
	SERC	0.75	0.93	0.72	1.04	0.77	0.92
	STEI	0.43	1.58	0.41	1.56	0.47	1.47
	UNDE	0.47	1.50	0.45	1.49	0.47	1.44
	WOMB	0.01	1.75	0.00	1.87	0.03	1.72

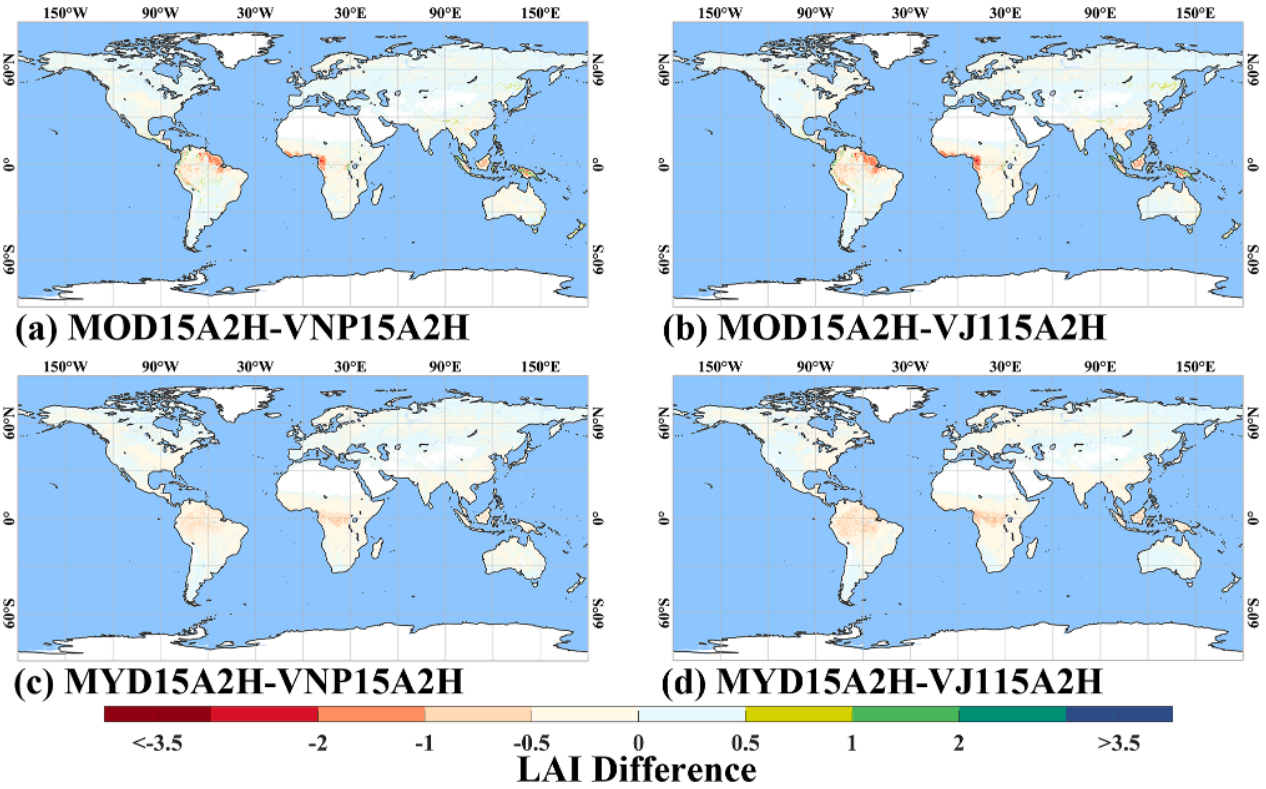


FIGURE 23.5 The global distribution of annual average LAI difference (MODIS-VIIRS) for year 2023. (a) Displays the difference between MOD15A2H C61 and VNP15A2H C2, while panel (b) Shows the difference between MYD15A2H C61 and VNP15A2H C2. (c) Displays the difference between MOD15A2H C61 and VJ115A2H C2, while panel (d) Shows the difference between MYD15A2H C61 and VJ115A2H C2. ***Map lines delineate study areas and do not necessarily depict accepted national boundaries.***

patterns of annual average LAI differences between MODIS and VIIRS products over 2023. The corresponding FPAR differences are shown in Fig. 23.6. In general, the overall differences between LAI and FPAR for both sensors are within ±0.5 for about 94.50% of retrievals and within ±0.1 for about 98.22%, with larger differences over dense forests. In general, MODIS and VIIRS show a high consistency, which is also demonstrated by the low percentage of pixels that differ significantly. The percentage of LAI differences above ±1 ranges from 0.11%–2.45% and the corresponding percentage for FPAR differences over ±0.2 are both less than 0.72%.

Fig. 23.7a and b illustrates the global distribution of absolute LAI differences between MOD15A2H C61 and two other open public LAI products in 2001, while Fig. 23.7c and d shows FPAR differences. Overall, the products exhibit continuous LAI/FPAR distributions globally. MODIS shows significant underestimation in dense tropical forests (e.g., Amazon and South Asia) compared to GLASS and GIMMS. This is due to MODIS always tends to use backup retrievals caused by rainy season-related cloud cover. GLASS and GIMMS avoid underestimates through gap-filling method. MODIS agrees better with GLASS than GIMMS, with absolute LAI differences under 1 for most regions (11.13% for GLASS vs. 14.20% for GIMMS). The overall differences between FPAR for MODIS and GLASS are within ±0.1 for about 93.20%, which is higher than the number 91.33% for GIMMS. This is due to GLASS using the MODIS reflectance as input and using the MODIS LAI/FPAR product in the GLASS retrieval algorithm for training. In addition, the difference in FPAR between MODIS and GIMMS is more pronounced at higher latitudes; the MODIS FPAR is directly influenced by incident solar radiation, especially in high-latitude regions.

5. Product applications

The MODIS&VIIRS LAI/FPAR products provide valuable parameters needed for understanding the global vegetation cover dynamics over a span of more than 20 years. Through the study of all over the world, this product sheds

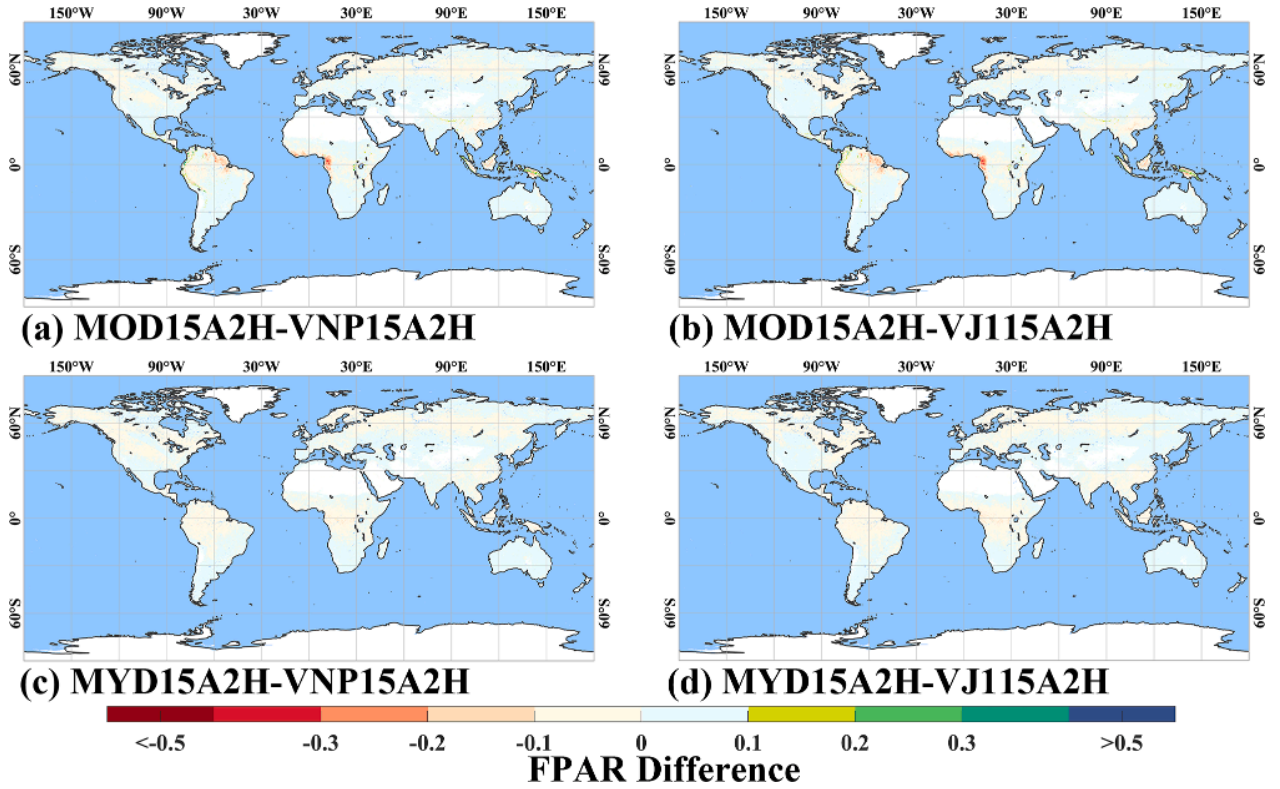


FIGURE 23.6 Same as Fig. 23.5 but for FPAR. The global distribution of annual average FPAR difference (MODIS-VIIRS) for year 2023. ***Map lines delineate study areas and do not necessarily depict accepted national boundaries.***

light on the relationship between vegetation change and the influence of climate. In addition, the LAI/FPAR product serves as a valuable tool for exploring the global carbon cycle by analyzing vegetation response to climate. And these products will be utilized to gain a deeper understanding of several important topics. I will provide some key examples of research based on this MODIS&VIIRS LAI/FPAR products as follows:

1) Greening Earth: Previous studies identified a global greening trend in vegetation (Zhang et al., 2017; Chen et al., 2019). Using MOD15A2H C61 LAI/FPAR data (2001–23), this part confirms the greening trend. Results show 39.78% of vegetated areas greening and 11.84% browning based on LAI, with FPAR indicating similar proportions (40.01% greening, 10.55% browning) (Fig. 23.8a and b). Globally, vegetation greenness has increased significantly, with LAI and FPAR trends of 1.19% and 1.26% per decade, respectively, suggesting a net rise in leaf area. Regionally, China and India are major contributors to this trend, while browning is observed in high latitudes, southern Africa, and parts of the Amazon. These findings align with those of Chen et al. (2019), further supporting the observed trends.
2) Inputs used as benchmarks for other global products: The same type of global LAI/FPAR products are often based on MODIS&VIIRS LAI/FPAR products for training and incorporating other data to generate similar products, for example, GLASS LAI/FPAR; GLOBMAP LAI; GIMMS LAI4g; GIMMS FPAR4g; sensor-independent LAI/FPAR CDR, etc (Liang et al., 2013; Deng et al., 2006; Cao et al., 2023; Zhao et al., 2024; Pu et al., 2024). The MODIS&VIIRS GPP/NPP products used MODIS&VIIRS LAI/FPAR products as input for production efficiency model, which can help to quantify the largest carbon flux in earth system (Running and Zhao, 2015). The MODIS&VIIRS FPAR product provides the basis for some light use efficiency-based models to estimate GPP/NPP (Running and Zhao, 2015; Endsley et al., 2023). And the MODIS&VIIRS LAI product offers the possibility for models to take leaf condition into account (Zheng et al., 2020). The datasets calculated above are also widely used in crop yield estimation, vegetation phenology analysis, and ecological environment analysis (Doraiswamy et al., 2005; Ahl et al., 2006; Bojinski et al., 2014).
3) Carbon cycle: The above products allow scientists to assess how ecosystems absorb and store atmospheric

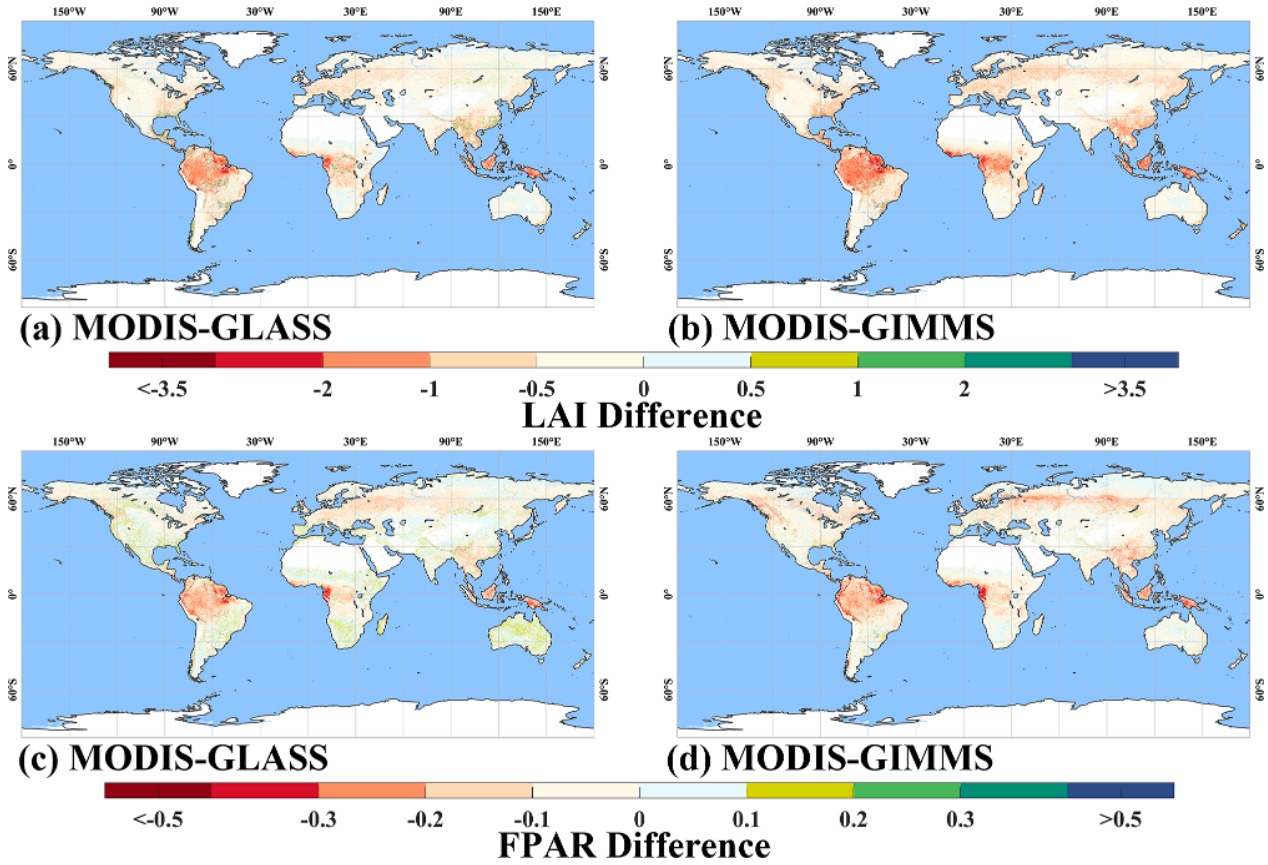


FIGURE 23.7 Global distribution of absolute differences between (a) MODIS and GLASS LAI; (b) MODIS and GIMMS LAI; (c) MODIS and GLASS FPAR; (d) MODIS and GIMMS FPAR in 2001. The spatial resolution is 0.05 degrees. The MODIS LAI/FPAR refers to MOD15A2H C61 LAI/FPAR and GIMMS LAI/FPAR means GIMMS LAI4g/FPAR4g. ***Map lines delineate study areas and do not necessarily depict accepted national boundaries.***

carbon dioxide, as well as how vegetation responds to seasonal, interannual, and long-term climate changes (Ahl et al., 2006; Tang et al., 2013; Zhu et al., 2016). For example, long-term LAI/FPAR data have been used to monitor the effects of droughts, wildfires, and land-use changes, such as deforestation or reforestation, on carbon sequestration (Skidmore and Pettorelli, 2015; Zhu et al., 2016; Chen et al., 2019). Additionally, they play a crucial role in global carbon budget studies, supporting Earth system models to quantify regional and global carbon fluxes more accurately (Winkler et al., 2021, 2024). Moreover, the availability of consistent, long-term datasets spanning over 2 decades enables researchers to explore trends and predict future scenarios under varying climate and land-use conditions, contributing to global carbon monitoring programs and informing sustainable management practices (Hu et al., 2022).

4) Energy balance: Based on some previous studies, an increase in LAI leads to evapotranspiration from the surface, which increases latent heat flux and decreases sensible heat flux (Forzieri et al., 2020). MODIS LAI product help to quantify this point, where a unit change in LAI leads to an increase in latent and decrease in sensible heat fluxes of 3.66 and -3.26 W/m^2, respectively. In addition, MODIS LAI products are also used to analyze the internal causes of global urban heat island phenomena based on the principle of energy balance (Chen et al., 2021).

6. Product availability

The MOD15A2H/MYD15A2H Version 6.1 and the VNP15A2H Version 2 Level 4 land products are available on https://ladsweb.modaps.eosdis.nasa.gov/ (accessed on Nov 15, 2024).

TABLE 23.3 Same as Table 23.2 but for FPAR, comparison of MODIS FPAR and VIIRS FPAR over GBOV sites.

Biome type	Site	R^2 MOD	RMSE MOD	R^2 MYD	RMSE MYD	R^2 VNP	RMSE V
Grasslands	CPER	0.75	0.17	0.72	0.17	0.71	0.17
	KONA	0.88	0.15	0.87	0.15	0.88	0.16
	MOAB	0.06	0.13	0.04	0.13	0.05	0.13
	ONAQ	0.50	0.14	0.43	0.14	0.44	0.14
	SPER	0.69	0.15	0.72	0.14	0.71	0.13
	STER	0.74	0.15	0.74	0.15	0.73	0.15
	WOOD	0.79	0.17	0.78	0.17	0.78	0.18
Forests	HARV	0.48	0.18	0.39	0.20	0.46	0.18
	TALL	0.33	0.11	0.37	0.10	0.50	0.09
	TUMB	0.26	0.16	0.39	0.16	0.34	0.14
Grass and shrubs	JORN	0.55	0.14	0.57	0.14	0.56	0.15
	VALE	0.09	0.13	0.11	0.12	0.09	0.13
Crops and savannas	BLAN	0.57	0.12	0.46	0.13	0.51	0.12
	LAJA	0.67	0.11	0.51	0.11	0.63	0.10
Grass and savannas	GUAN	0.68	0.09	0.50	0.10	0.66	0.08
	JERC	0.46	0.13	0.40	0.14	0.49	0.14
	LITC	0.27	0.18	0.07	0.18	0.02	0.19
	NIWO	0.02	0.23	0.02	0.23	0.01	0.24
Savannas and forests	BART	0.39	0.23	0.36	0.24	0.39	0.23
	DELA	0.74	0.12	0.69	0.13	0.76	0.14
	DSNY	0.07	0.17	0.02	0.20	0.08	0.16
	HAIN	0.50	0.18	0.65	0.16	0.63	0.16
	ORNL	0.72	0.12	0.67	0.14	0.77	0.11
	OSBS	0.01	0.10	0.01	0.12	0.02	0.10
	SCBI	0.86	0.12	0.78	0.14	0.90	0.10
	SERC	0.78	0.12	0.74	0.13	0.79	0.12
	STEI	0.11	0.34	0.09	0.35	0.15	0.30
	UNDE	0.18	0.34	0.17	0.34	0.20	0.31
	WOMB	0.00	0.11	0.00	0.15	0.00	0.14

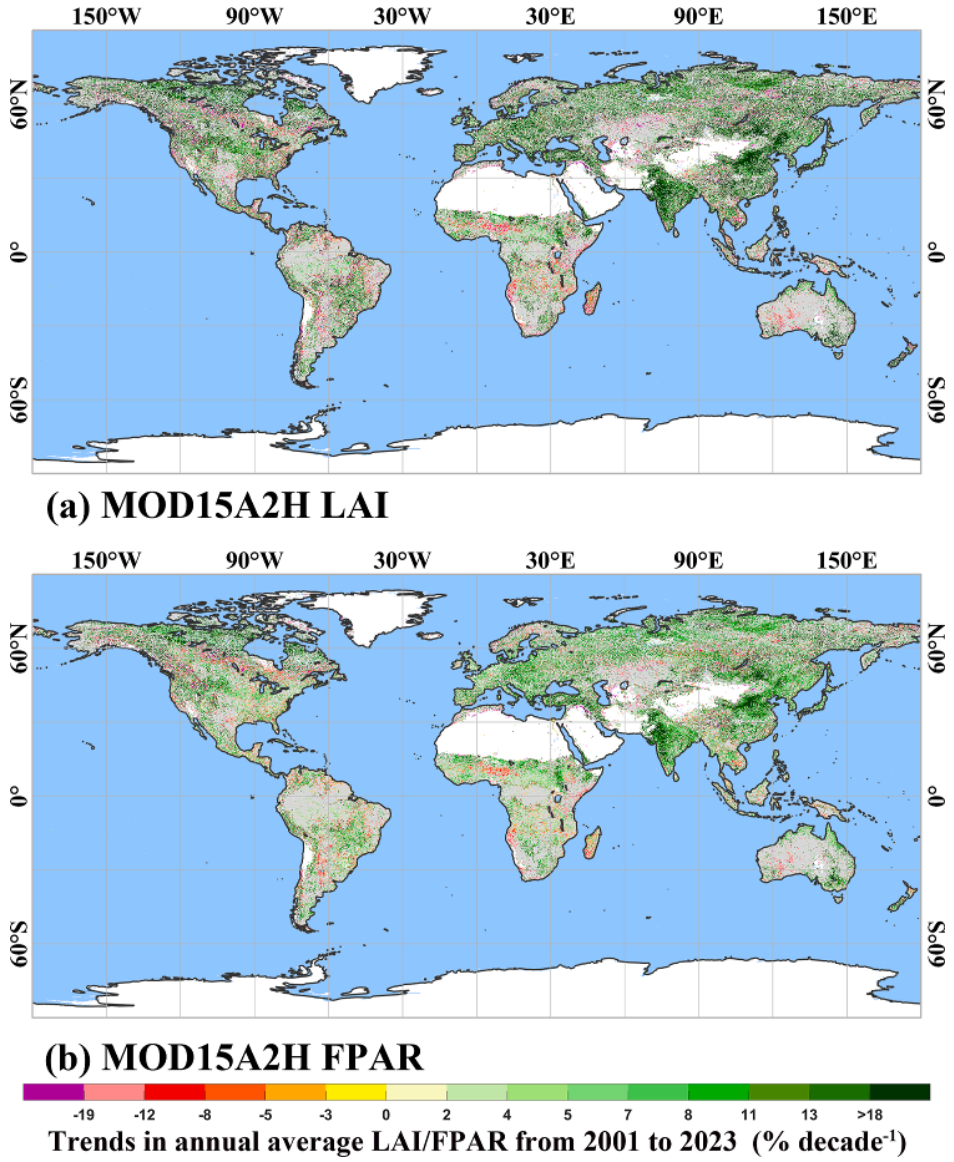


FIGURE 23.8 Map of trends in annual average MOD15A2H LAI/FPAR for 2001–23. Statistically significant trends (Mann–Kendall test; $P \leq .1$) are color coded. Gray areas show vegetated land with statistically insignificant trends. White areas depict barren lands, permanent ice-covered areas, permanent wetlands, and built-up areas. Blue areas represent water. ***Map lines delineate study areas and do not necessarily depict accepted national boundaries.***

References

Ahl, D.E., Gower, S.T., Burrows, S.N., Shabanov, N.V., Myneni, R.B., Knyazikhin, Y., 2006. Monitoring spring canopy phenology of a deciduous broadleaf forest using MODIS. Rem. Sens. Environ. 104 (1), 88–95.

Bojinski, S., Verstraete, M., Peterson, T.C., Richter, C., Simmons, A., Zemp, M., 2014. The concept of essential climate variables in support of climate research, applications, and policy. Bull. Am. Meteorol. Soc. 95 (9), 1431–1443.

Brown, L.A., Meier, C., Morris, H., Pastor-Guzman, J., Bai, G., Lerebourg, C., et al., 2020. Evaluation of global leaf area index and fraction of absorbed photosynthetically active radiation products over North America using Copernicus Ground Based Observations for Validation data. Rem. Sens. Environ. 247, 111935.

Brown, L.A., Camacho, F., García-Santos, V., Origo, N., Fuster, B., Morris, H., et al., 2021. Fiducial reference measurements for vegetation bio-geophysical variables: an end-to-end uncertainty evaluation framework. Remote Sens. 13 (16), 3194.

Cao, S., Li, M., Zhu, Z., Wang, Z., Zha, J., Zhao, W., et al., 2023. Spatiotemporally consistent global dataset of the GIMMS leaf area index (GIMMS LAI4g) from 1982 to 2020. Earth Syst. Sci. Data 15 (11), 4877–4899.

Chen, C., Park, T., Wang, X., Piao, S., Xu, B., Chaturvedi, R.K., et al., 2019. China and India lead in greening of the world through land-use management. Nat. Sustain. 2 (2), 122–129.

Chen, C., Knyazikhin, Y., Park, T., Yan, K., Lyapustin, A., Wang, Y., et al., 2017. Prototyping of LAI and FPAR retrievals from MODIS multi-angle implementation of atmospheric correction (MAIAC) data. Remote Sens. 9 (4), 370.

Chen, C., Li, D., Keenan, T.F., 2021. Enhanced surface urban heat islands due to divergent urban-rural greening trends. Environ. Res. Lett. 16 (12), 124071.

Chen, C., Riley, W.J., Prentice, I.C., Keenan, T.F., 2022. CO_2 fertilization of terrestrial photosynthesis inferred from site to global scales. Proc. Natl. Acad. Sci. 119 (10), e2115627119.

Chen, J.M., Black, T.A., 1992. Defining leaf area index for non-flat leaves. Plant Cell Environ. 15 (4), 421–429.

Deng, F., Chen, J.M., Plummer, S., Chen, M., Pisek, J., 2006. Algorithm for global leaf area index retrieval using satellite imagery. IEEE Trans. Geosci. Rem. Sens. 44 (8), 2219–2229.

Doraiswamy, P.C., Sinclair, T.R., Hollinger, S., Akhmedov, B., Stern, A., Prueger, J., 2005. Application of MODIS derived parameters for regional crop yield assessment. Rem. Sens. Environ. 97 (2), 192–202.

Endsley, K.A., Zhao, M., Kimball, J.S., Devadiga, S., 2023. Continuity of global MODIS terrestrial primary productivity estimates in the VIIRS era using model-data fusion. J. Geophys. Res.: Biogeosciences 128 (9), e2023JG007457.

Forzieri, G., Miralles, D.G., Ciais, P., Alkama, R., Ryu, Y., Duveiller, G., et al., 2020. Increased control of vegetation on global terrestrial energy fluxes. Nat. Clim. Change 10 (4), 356–362.

Ganguly, S., Schull, M.A., Samanta, A., Shabanov, N.V., Milesi, C., Nemani, R.R., et al., 2008a. Generating vegetation leaf area index earth system data record from multiple sensors. Part 1: theory. Rem. Sens. Environ. 112 (12), 4333–4343.

Ganguly, S., Samanta, A., Schull, M.A., Shabanov, N.V., Milesi, C., Nemani, R.R., et al., 2008b. Generating vegetation leaf area index Earth system data record from multiple sensors. Part 2: implementation, analysis and validation. Rem. Sens. Environ. 112 (12), 4318–4332.

GCOS, 2011. Systematic Observation Requirements for Satellite-Based Products for Climate, 2011 Update, Supplemental Details to the Satellite-Based Component of the Implementation Plan for the Global Observing System for Climate in Support of the UNFCCC (2010 Update). GCOS-154, p. 138. https://library.wmo.int/doc_num.php?explnum_id=3710.

GCOS, 2016. The Global Observing System for Climate: Implementation Needs. GCOS-200. https://unfccc.int/sites/default/files/gcos_ip_10oct2016.pdf.

Hu, Q., Li, T., Deng, X., Wu, T., Zhai, P., Huang, D., et al., 2022. Intercomparison of global terrestrial carbon fluxes estimated by MODIS and Earth system models. Sci. Total Environ. 810, 152231.

Justice, C.O., Roman, M.O., Csiszar, I., Vermote, E.F., Wolfe, R.E., Hook, S.J., et al., 2013. Land and cryosphere products from Suomi NPP VIIRS: overview and status. J. Geophys. Res. Atmos. 118 (17), 9753–9765.

Knyazikhin, Y., Martonchik, J.V., Myneni, R.B., Diner, D.J., Running, S. W., 1998. Synergistic algorithm for estimating vegetation canopy leaf area index and fraction of absorbed photosynthetically active radiation from MODIS and MISR data. J. Geophys. Res. Atmos. 103 (D24), 32257–32275.

Knyazikhin, Y., 1999. MODIS Leaf Area Index (LAI) and Fraction of Photosynthetically Active Radiation Absorbed by Vegetation (FPAR) Product (MOD15) Algorithm Theoretical Basis Document. https://modis.gsfc.nasa.gov/data/atbd/atbd_mod15.pdf.

Knyazikhin, Y., Myneni, R., 2018. VIIRS Leaf Area Index (LAI) and Fraction of Photosynthetically Active Radiation Absorbed by Vegetation (FPAR) User Guide. https://lpdaac.usgs.gov/documents/126/VNP15_User_Guide.pdf.

Liang, S., Zhao, X., Liu, S., Yuan, W., Cheng, X., Xiao, Z., et al., 2013. A long-term Global LAnd Surface Satellite (GLASS) data-set for environmental studies. Int. J. Digit. Earth 6 (Suppl. 1), 5–33.

Mariano, D.A., dos Santos, C.A., Wardlow, B.D., Anderson, M.C., Schiltmeyer, A.V., Tadesse, T., Svoboda, M.D., 2018. Use of remote sensing indicators to assess effects of drought and human-induced land degradation on ecosystem health in Northeastern Brazil. Rem. Sens. Environ. 213, 129–143.

Myneni, R.B., Hoffman, S., Knyazikhin, Y., Privette, J.L., Glassy, J., Tian, Y., et al., 2002. Global products of vegetation leaf area and fraction absorbed PAR from year one of MODIS data. Rem. Sens. Environ. 83 (1–2), 214–231.

Myneni, R.B., Park, T., 2015. MODIS Collection 6 (C6) LAI/FPAR Product User's Guide. https://modis-land.gsfc.nasa.gov/pdf/MOD15_C6_UserGuide_June2020.pdf.

Pu, J., Yan, K., Roy, S., Zhu, Z., Rautiainen, M., Knyazikhin, Y., Myneni, R.B., 2024. Sensor-independent LAI/FPAR CDR: reconstructing a global sensor-independent climate data record of MODIS and VIIRS LAI/FPAR from 2000 to 2022. Earth Syst. Sci. Data 16 (1), 15–34.

Running, S.W., Zhao, M., 2015. Daily GPP and annual NPP (MOD17A2/A3) products NASA Earth Observing System MODIS land algorithm. In: MOD17 User's Guide, 2015, pp. 1–28.

Roman, M.O., Justice, C., Paynter, I., Boucher, P.B., Devadiga, S., Endsley, A., et al., 2024. Continuity between NASA MODIS collection 6.1 and VIIRS collection 2 land products. Rem. Sens. Environ. 302, 113963.

Skidmore, A.K., Pettorelli, N., 2015. Agree on biodiversity metrics to track from space: ecologists and space agencies must forge a global monitoring strategy. Nature 523 (7561), 403–406.

Tang, X., Wang, Z., Xie, J., Liu, D., Desai, A.R., Jia, M., et al., 2013. Monitoring the seasonal and interannual variation of the carbon sequestration in a temperate deciduous forest with MODIS time series data. For. Ecol. Manag. 306, 150–160.

Winkler, A.J., Myneni, R.B., Hannart, A., Sitch, S., Haverd, V., Lombardozzi, D., et al., 2021. Slowdown of the greening trend in natural vegetation with further rise in atmospheric CO_2. Biogeosciences 18 (17), 4985–5010.

Winkler, A.J., Myneni, R., Reimers, C., Reichstein, M., Brovkin, V., 2024. Carbon system state determines warming potential of emissions. PLoS One 19 (8), e0306128.

Xu, B., Park, T., Yan, K., Chen, C., Zeng, Y., Song, W., et al., 2018. Analysis of global LAI/FPAR products from VIIRS and MODIS sensors for spatio-temporal consistency and uncertainty from 2012–2016. Forests 9 (2), 73.

Yan, K., Park, T., Chen, C., Xu, B., Song, W., Yang, B., et al., 2018. Generating global products of LAI and FPAR from SNPP-VIIRS data: theoretical background and implementation. IEEE Trans. Geosci. Rem. Sens. 56 (4), 2119–2137.

Yan, K., Park, T., Yan, G., Chen, C., Yang, B., Liu, Z., et al., 2016a. Evaluation of MODIS LAI/FPAR product collection 6. Part 1: consistency and improvements. Remote Sens. 8 (5), 359.

Yan, K., Park, T., Yan, G., Liu, Z., Yang, B., Chen, C., et al., 2016b. Evaluation of MODIS LAI/FPAR product collection 6. Part 2: validation and intercomparison. Remote Sens. 8 (6), 460.

Yan, K., Pu, J., Park, T., Xu, B., Zeng, Y., Yan, G., et al., 2021. Performance stability of the MODIS and VIIRS LAI algorithms inferred from analysis of long time series of products. Rem. Sens. Environ. 260, 112438.

Yang, W., Huang, D., Tan, B., Stroeve, J.C., Shabanov, N.V., Knyazikhin, Y., et al., 2006. Analysis of leaf area index and fraction of PAR absorbed by vegetation products from the terra MODIS sensor: 2000-2005. IEEE Trans. Geosci. Rem. Sens. 44 (7), 1829–1842.

Zhang, Y., Song, C., Band, L.E., Sun, G., Li, J., 2017. Reanalysis of global terrestrial vegetation trends from MODIS products: browning or greening? Rem. Sens. Environ. 191, 145–155.

Zhao, W., Zhu, Z., Cao, S., Li, M., Zha, J., Pu, J., Myneni, R.B., 2024. A global dataset of the fraction of absorbed photosynthetically active radiation for 1982–2022. Sci. Data 11 (1), 707.

Zheng, Y., Shen, R., Wang, Y., Li, X., Liu, S., Liang, S., et al., 2020. Improved estimate of global gross primary production for reproducing its long-term variation, 1982–2017. Earth Syst. Sci. Data 12 (4), 2725–2746.

Zhu, Z., Piao, S., Myneni, R.B., Huang, M., Zeng, Z., Canadell, J.G., et al., 2016. Greening of the earth and its drivers. Nat. Clim. Change 6 (8), 791–795.